

# Fabrication and Potential Characterization of Silver-Doped Zinc Oxide Glucose Biosensor

Muhammad Junaid,\* Avimra Haleema, Raheela Jabeen,\* Mahmood Basil A. AL-Rawi, Mohammed El-Meligy, and Sibtain Ahmed

This work is devoted to studying and manufacturing a highly sensitive nonenzymatic glucose biosensing system of metal oxides via the sol-gel technique. The X-ray diffraction patterns of all the prepared samples confirm that the samples present hexagonal crystal lattice structures of ZnO and Ag-ZnO nanoparticles. Ultraviolet (UV) analysis of all the samples is carried out to evaluate the absorption of silver in the UV region for electrical and chronoamperometric analysis. The transmittance of all the samples is observed, and the maximum transmittance is 11% for 4% AgZnO. Fourier transform infrared spectroscopy reveal the functional group stretching and vibration of the particles at different wavelength ranges. Scanning electron microscopy analysis reveals the grain size and morphology of the samples, which decrease with increasing doping agent. Chronoamperometric analysis of all the samples reveals that the value increases with time for the 4% doped sample. The sensing response is also observed and is enhanced with increasing temperature for the 4% doped sample. The sensing response of the samples coated with carbon fiber electrodes is assessed from  $-0.2$  to  $+0.5$  V at a scan rate of  $50$  mV s<sup>-1</sup>.

instance, the nanoscale encourages better signal transduction. Also, it increases the surface area for the reaction of biomolecules. The evolution of glucose nanobiosensors estimates the sugar levels at miniaturization power.<sup>[2]</sup> Nanoscale targeting of glucose facilitates real-time detection. In recent years, metal oxides have given a lot of advantages in nanotechnology. Metals have advantageous conducting, catalytic, optic, and electronic properties that facilitate biosensing.<sup>[3]</sup> The applications of metal oxides include the fabrication of microelectronic circuits, sensors, piezoelectric devices, and nanostructures with remarkable potential and extraordinary properties. A group of nanoparticles, metal oxide nanoparticles (MO-NPs), hold much importance in modern nanotechnology-based sensors and medicine. Its superparamagnetic behavior, exclusive catalytic activity, selectivity, and

## 1. Introduction

The inclusion of nanotechnology has revolutionized the path of developing electrical gadgets and composites.<sup>[1]</sup> Nanoparticle-based biosensors are state-of-the-art gadgets that measure the minimal content of analyte in the sample. The nanophase complexes have many exceptional features due to which they serve as remarkable contrivances in modern nanotechnologies. For

sensitivity<sup>[4]</sup> vitally improve the sustainability and fidelity of the next-generation sensing tools. Moreover, zinc oxide nanoparticles (ZnO-NPs) are a type of metal oxide nanoparticles that are extensively used as semiconductor oxide<sup>[5]</sup> in various gadgets. This semiconductor is typically doped with conductor metals like silver (Ag) to enhance their functioning features (electric, optic, and catalytic), reduce bandgap for quick response, and produce stability in strong electrolytes.<sup>[6]</sup> Based on this, Ag doping of

M. Junaid  
Institute of Physics  
The Islamia University of Bahawalpur  
Bahawalpur 63100, Pakistan  
E-mail: mjunaid310@yahoo.com

A. Haleema, R. Jabeen  
Department of Biochemistry and Biotechnology  
The Women University Multan  
Multan 6000, Pakistan  
E-mail: drraheela.9054@wum.edu.pk

M. B. A. AL-Rawi  
Department of Optometry  
College of Applied Medical Sciences  
King Saud University  
PO Box 366, Riyadh 11481, Saudi Arabia

 The ORCID identification number(s) for the author(s) of this article can be found under <https://doi.org/10.1002/pssa.202400817>.

M. El-Meligy  
Jadara University Research Centre  
Jadara University  
PO Box 733, Ibrid, Jordan

M. El-Meligy  
Applied Science Research Center  
Applied Science Private University  
Amman, Jordan

S. Ahmed  
Scripps Institution of Oceanography  
University of California San Diego  
9500 Gilman Drive, La Jolla, CA 92093, USA

S. Ahmed  
Department of Biochemistry  
Bahauddin Zakariya University  
Multan 60800, Pakistan

DOI: 10.1002/pssa.202400817

ZnO-NPs has been performed to enhance the functioning potential of ZnO-NPs in the present work. The sol-gel method has been chosen for the preparation of Ag-doped ZnO nanoparticles due to its simple operation, mild conditions, and excellent crystalline shape of particles.<sup>[7]</sup> The use of enzyme-based glucose biosensors has been discouraged recently due to demanding operating conditions for enzymes and various other drawbacks including high cost and limited actions. Metal oxide electrodes are used instead of enzymes in biosensors nowadays. Redox properties of metal oxide (ZnO) offer an alternative way to glucose sensing. However, a nonenzymatic amperometric system developed in this research wherein metal (Ag)-doped metal oxide (ZnO) nanoparticles made the working carbon electrode for glucose monitoring.<sup>[8]</sup> The redox features of ZnO have been leveraged for glucose detection by amperometric responses. These responses have been measured by an essential electrochemical process, chronoamperometry. In this process, the analyte (glucose) molecule is converted into an electrochemical signal in the presence of continuous voltage for a certain time frame.<sup>[9]</sup> Investigating the potential of the Ag-ZnO NPs is a valuable contribution to glucose sensing technology.

Diabetes is a global health challenge that has distressed millions of people globally.<sup>[1]</sup> Damage to the beta-cells of the pancreas alters glucose (sugar) metabolism within the body, resulting in organ dysfunction and eventually death.<sup>[2]</sup> The inclusion of nanotechnology has revolutionized the path of developing electrical devices and composites with diagnostic importance.<sup>[6]</sup> Metal oxide nanoparticles (MO-NPs), a group of nanoparticles, are remarkable contributors to modern nanotechnology-based sensors and medicine.<sup>[7]</sup> This is because of their extraordinary superparamagnetic behavior, exclusive catalytic activity, selectivity, and sensitivity.<sup>[8]</sup> ZnO is a broadly used semiconductor oxide<sup>[9]</sup> that is generally doped with conductor metals (Ag) to enhance its functional features (electric, optic, and catalytic), reduce the bandgap for quick response, and produce stability in strong electrolytes.<sup>[10]</sup> However, Ag doping of ZnO-NPs was performed in this study. The demanding operating conditions for enzymes, along with various other drawbacks, discourage the use of enzyme-based glucose biosensors. In the present work, a nonenzymatic amperometric glucose biosensor was developed by using metal (Ag) oxide (ZnO) nanoparticles (prepared via the sol-gel method) to make a working carbon electrode for glucose monitoring.<sup>[11]</sup> Sol-gel preparation has been chosen because of its simple operation, mild conditions, and excellent crystalline shape of the particles.<sup>[12]</sup> In this work, the redox properties of a metal oxide (ZnO) offer an alternative way to sense glucose. The redox features of ZnO have been leveraged for glucose detection via amperometric responses. A broadly used electrochemical method, chronoamperometry, was adopted for amperometric detection. In this method, the analyte (glucose) molecule is converted into an electrochemical signal at a continuous voltage for a specific time frame.

## 2. Methodology

### 2.1. Synthesis of Ag-doped ZnO-NPs

An appropriate amount of zinc acetate dihydrate ( $\text{ZnC}_4\text{H}_6\text{O}_4 \cdot 2\text{H}_2\text{O}$ , AnalaR) and a stock solution of NaOH were used to

**Table 1.** Description of the prepared samples.

Sr. #	Sample name	Zinc acetate ( $\text{ZnC}_4\text{H}_6\text{O}_4 \cdot 2\text{H}_2\text{O}$ ) [g]	Dopant ( $\text{AgNO}_3$ ) content	Ag % in ZnO [%]
1	S1 (Pure ZnO-NPs)	4.5	0 g	0
2	S2 (2% Ag-ZnO-NPs)	4.5	20 mL of stock soln.	2
3	S3 (3% Ag-ZnO-NPs)	4.5	30 mL of stock soln.	3
4	S4 (4% Ag-ZnO-NPs)	4.5	40 mL of stock soln.	4

prepare a milky white solution on a hot plate stirrer for three successive hours.<sup>[13]</sup> Silver salt ( $\text{AgNO}_3$ ) was used as an Ag source for doping. Ag doping was performed at three different concentrations, 2%, 3%, and 4% by weight (wt%), by mixing suitable proportions of  $\text{AgNO}_3$  stock solution and ZnO milky white solution on a hot plate stirrer ( $\approx 3$  h, 42–45 °C). After preparation, the solution was dried at 90 °C for 2 h in a hot air oven. The dried materials were ground and calcined at 450 °C for 6 h in a furnace (Vulcan A-550) as shown in **Table 1**.

The particle size, distribution surface area, porosity, chemical composition, purity, crystal structure, phase, optical, electrical, and mechanical properties are affected when samples are prepared by sol-gel technique.

### 2.2. Characterization of Ag-doped ZnO-NPs

The detailed characterization (structure, composition, and chemical properties) of the doped and undoped ZnO nanoparticles was performed via Fourier transform infrared spectroscopy (FTIR), X-ray diffraction (XRD), ultraviolet (UV)-vis spectroscopy, scanning electron microscope (SEM), and chronoamperometric analysis. XRD was used to examine the crystallinity, purity, and crystallinity of the ZnO and Ag-ZnO nanoparticles. The structure and conformation of Ag-doped ZnO were verified by analyzing the FTIR spectra of the Ag-doped and undoped ZnO nanoparticles.<sup>[14]</sup> The optical properties of the prepared samples were assessed via absorbance measurements from a high-resolution UV-vis spectrophotometer in the range of 400–800 nm. SEM measurements were used for the morphological analysis of the sample.<sup>[14]</sup>

### 2.3. Preparation of Ag-ZnO Carbon-Pasted Electrodes

The prepared S1, S2, S3, and S4 samples were mixed with carbon paste ( $1:3 \text{ w w}^{-1}$ ) and placed onto the surface of the carbon fiber electrode separately to construct four working electrodes.<sup>[15]</sup>

### 2.4. Electrochemical Analysis of Beta-D-Glucose with Prepared Electrodes

KCl voltammetry was used to monitor the electrochemical behavior of the modified electrodes in the three-electrode system. The supporting electrolyte was KCl, the reference electrode was AgCl,

the counter electrode was a platinum (Pt) wire, and carbon-pasted Ag-doped and Ag-undoped ZnO-NPs were used as working electrodes. The electrochemical behavior of all the electrodes was examined in a 0.1 mol L<sup>-1</sup> KCl solution via chronoamperometry. The current response of each sample was recorded in the potential range between -0.2 and 0.5 V at 50 mVs<sup>-1</sup> scan rate. The electrocatalytic activity of the electrodes was investigated in the presence of 5 mM glucose and 1 mmol L<sup>-1</sup> H<sub>2</sub>O<sub>2</sub> in 0.1 mol L<sup>-1</sup> phosphate buffer solution (PBS, pH 7.0).<sup>[16]</sup> The glucose solution was sequentially added to the electrolyte solution during electrochemical analysis.

### 3. Results and Discussion

#### 3.1. XRD Outcomes of Pure and Ag-doped ZnO-NPs

The confirmation of ZnO and Ag-doped ZnO nanoparticles is analyzed through XRD using a Bruker D8 Advance powder X-ray diffractometer with Cu K $\alpha$  ( $\lambda = 1.5406 \text{ \AA}$ ) radiation. The presence of various symmetrical reflections in the diffraction pattern of ZnO (Figure 1) complements the wurtzite hexagonal phase, suggesting that the hexagonal crystal of ZnO is rather than cubic. The ZnO crystal phase is highly consistent with the XRD pattern of JCPDS card number 146-1451. The other reference code used for the analysis was 01-080-0075.<sup>[17,18]</sup> The peaks of the 4% Ag-ZnO-NPs, 3% Ag-ZnO-NPs, and 2% Ag-ZnO-NPs show good crystalline patterns.<sup>[19]</sup> The reflections of diffraction associated with impurities were not evident in the spectrum. Additionally, the exquisite reflections support the exceptional crystalline phase of the ZnO and Ag-ZnO-NPs.

Furthermore, the shift of the zinc oxide lattice toward higher 2 theta (degrees) values at regular intervals in S2, S3, and S4 was similar to the current XRD results as reported in Table 2. This finding indicated that increasing the silver content verified the productive integration of Ag into the zinc oxide structure. Silver doping increased the number of active sites in the crystal lattice of zinc oxide.<sup>[17-19]</sup>

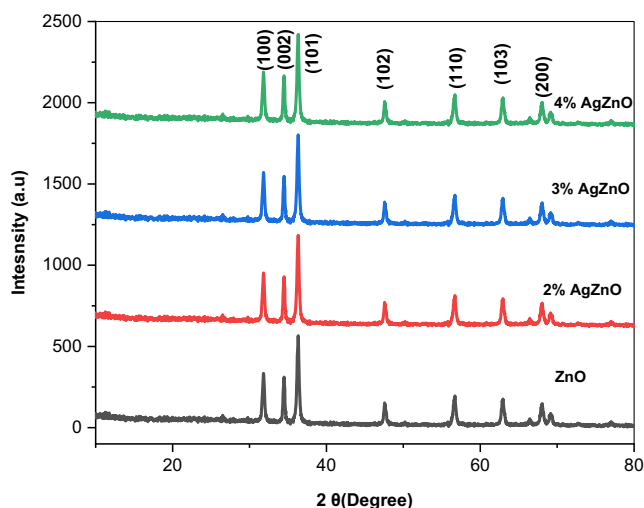


Figure 1. XRD study of ZnO and AgZnO.

Table 2. Comparison of the crystallite sizes obtained by XRD with crystallite sizes obtained by Scherrer's formula.

Crystallite size from XRD		Crystallite size from Scherrer formula	
ZnO	30.6 nm	ZnO	25.8 nm
2% Ag-doped ZnO	24.5 nm	2% Ag-doped ZnO	22.1 nm
3% Ag-doped ZnO	20.5 nm	3% Ag-doped ZnO	19.4 nm
4% Ag-doped ZnO	18.5 nm	4% Ag-doped ZnO	17.8 nm

#### 3.2. UV-Visible Analysis

A UV-vis-NIR spectrophotometer (Shimadzu UV2600 plus) equipped with an integrating sphere was used to assess the optical absorption and transmission of all prepared samples as shown in Figure 2. The maximum absorbance of ZnO is observed around 370 nm, which corresponds to the UV region. This is due to the bandgap energy of ZnO, which is  $\approx 3.37 \text{ eV}$  due to the energy corresponding to 360–380 nm matching the bandgap energy of ZnO, allowing electrons to transition from the valence band to the conduction band. ZnO has a high exciton binding energy ( $\approx 60 \text{ meV}$ ), leading to the formation of excitons (electron-hole pairs) at room temperature. These excitons contribute to the strong absorbance around 360–380 nm. ZnO nanoparticles exhibit quantum confinement effects, which enhance the absorbance due to increased oscillator strength ZnO's wurtzite crystal structure and lattice vibrations (phonons) also influence the absorbance spectrum.

Ag doping introduces localized surface plasmon resonance (LSPR) effects, leading to increased absorbance in the visible region 536 nm. The absorption peak in the UV region shifts to longer wavelengths (e.g., 380–400 nm) due to the introduction of Ag-related energy levels. Ag doping can enhance the absorbance intensity, particularly in the UV-vis region. As the doping increases from 2 to 3% and 4%, it is observed that absorbance increases in the visible region due to LSPR in the visible region

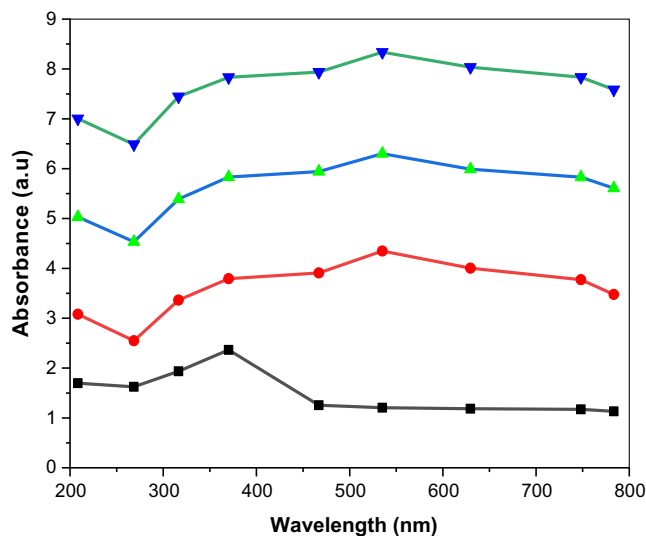


Figure 2. UV-absorption spectra of pure ZnO and Ag-doped ZnO.

(450–600 nm). LSPR enhances energy transfer from incident light to ZnO, increasing absorbance. LSPR-induced scattering localizes light within the ZnO matrix, prolonging interaction time and boosting absorbance. LSPR generates strong near-fields around Ag NPs, amplifying light-matter interactions.<sup>[18]</sup>

Four percent Ag doping levels can lead to increased LSPR effects and smaller particles ( $\approx 1\text{--}5$  nm) exhibit broader LSPR spectra. Enhanced visible light absorbance improves photocatalytic activity. Its increased absorbance boosts photovoltaic performance. The absorption of spectrum revealed that a sample with a high silver concentration (4% Ag-ZnO-NPs) has high optoelectronic properties, whereas a sample with a low silver concentration (2% Ag-ZnO-NPs) has less significant optical properties in the UV region.

Moreover, the optical and electrocatalytic properties were substantially enhanced by the high concentration of silver in the ZnO structure. This inference is correlated with the absorbance spectrum of our study; the peak of the 4% dopant appears higher than that of the ZnO structure, which is 2% and 3% dopant in concentration.<sup>[19,20]</sup>

### 3.3. Transmittance

The transmittance of ZnO is high and noted to be 23% in the visible region at the range of wavelength of 450 nm, whereas it decreases with increasing Ag concentration for 2% Ag-ZnO, 3% Ag-ZnO, and 4% Ag-ZnO showing 21%, 15%, and 8%, respectively, for the 4% as observed in **Figure 3**. This decreased level of transparency suggests that the sample has excellent optical quality as mentioned in **Figure 3**.

Increasing Ag concentration in ZnO can significantly impact its transmittance. Ag nanoparticles can absorb light, reducing transmittance, especially in the visible region. The increased Ag concentration can shift the absorption edge toward longer wavelengths, affecting transmittance, as Ag nanoparticles can scatter light, reducing transmittance.

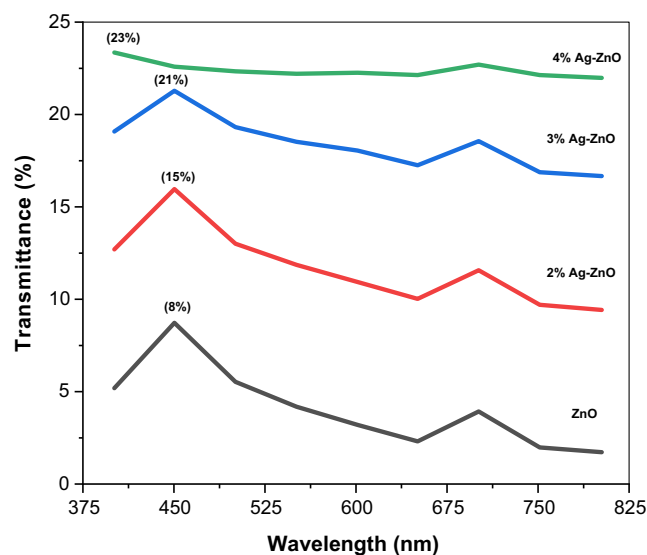


**Figure 3.** Transmittance of ZnO and Ag-ZnO.

The Ag nanoparticles absorb light, reducing transmission. Ag nanoparticles scatter light, reducing transmission. Excessive Ag doping can introduce defects, reducing transmittance. Ag doping can reduce ZnO's optical bandgap, affecting transmittance.

### 3.4. FTIR Analysis

The chemical conformations of the all-prepared samples were determined via FTIR spectroscopy (Thermo Scientific Nicolet iS 5 USA) as shown in **Figure 4**. The spectroscopy was carried out at wavenumbers ranging from 500 to 40 000  $\text{cm}^{-1}$ . The acute peak of pure zinc oxide was observed at 564  $\text{cm}^{-1}$ . The peaks of 2% Ag-ZnO-NPs, 3% Ag-ZnO, and 4% Ag-ZnO exhibited somewhat similar patterns.<sup>[17]</sup> Similarly, for the ZnO sample, sharp peaks at 1090  $\text{cm}^{-1}$  were observed for the 2% and 3% doped samples. A broad peak was observed at 1540  $\text{cm}^{-1}$  due to the bending vibration of H<sub>2</sub>O. This inference supported the previously reported literature that silver as a dopant did not impact the hydrophilic character of pure zinc oxide nanoparticles.<sup>[21]</sup> The presence of additional phases or impurities has been reported in 3% and 4% doped samples; the difference in pattern is due to the further phases of the AgO/AgO<sub>2</sub> or impure samples.<sup>[19]</sup> Ag doping affected the bond length and caused slight variations in the peaks of the FTIR spectra. The poor stretching and vibration in the IR region of the spectra were due to decreased bond length as shown in **Figure 4**.

### 3.5. SEM Analysis

The SEM (Cube II Emcraft South Korea) setup is used to analyze the morphology which is relatively arranged, along with a high degree of sample agglomeration. Clusters of minute nanoparticles were observed in each sample. The structures of the 4% Ag-doped, 3% Ag-doped, and 2% Ag-doped samples appeared as clusters of tiny hexagonal-shaped nanorods, indicating their relevance to the XRD results of the samples. The head-to-head

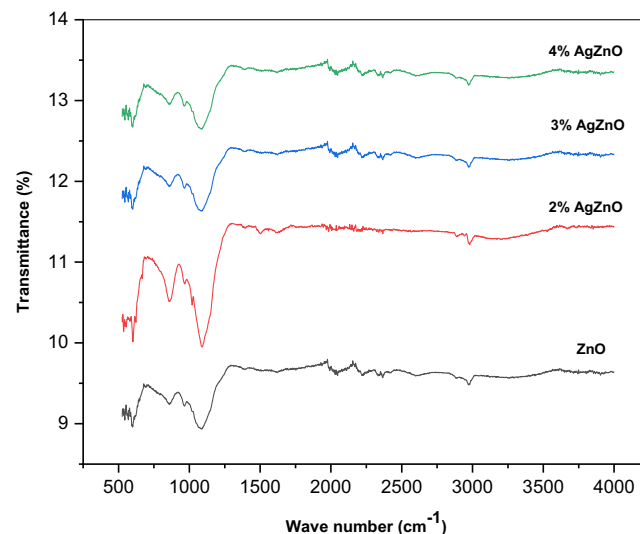


**Figure 4.** FTIR analysis of ZnO and Ag-doped ZnO.

and side-to-side fusion of the nanoparticles resulted in clusters of particles. The integration of the doped material did not readily influence the morphology of ZnO. Ag doping increased the asymmetry of the nanoparticles and resulted in agglomeration. However, a somewhat different morphology was observed for the 4% Ag-doped sample. Symmetrically organized hexagonal nanorods were observed. The presence of agglomeration in the particles and various crystallites highlights the poor crystallinity but does not influence the dimension of the particles.<sup>[20]</sup> The particles were held together by weak forces in all the samples, and these outcomes corroborated those of the present study.<sup>[12,14]</sup> Silver doping did not result in any substantial change in the structure of the particles, and the crystallite dimensions of the pure and doped samples in the SEM images remained the same as reported in **Figure 5**.

The grain size of all the samples was measured through ImageJ software, and a decrease in the grain size was found with increasing doping agent. Increased Ag doping decreases the bandgap energy, shifting the absorption edge toward the visible region. Higher Ag doping concentrations increase absorption in the visible range, making it suitable for photocatalytic applications. Ag doping enhances the electrical conductivity of ZnO through the introduction of extra electrons. Higher Ag doping

concentrations lead to an increase in the carrier concentration, affecting the electrical behavior of the material. Ag doping improves the photocatalytic efficiency of ZnO, especially for visible-light-driven reactions. Higher Ag doping concentrations can increase ROS production, enhancing photocatalytic activity. Ag doping can decrease the grain size, resulting in an increased surface area and improved photocatalytic activity. Higher Ag doping concentrations can cause changes in the crystal structure, potentially leading to increased defects and enhanced photocatalytic performance as mentioned in **Figure 6**. Ag doping can impart antibacterial properties to ZnO, making it suitable for biomedical applications. Higher Ag doping concentrations can affect the material's stability, potentially leading to increased degradation or oxidation.

### 3.6. Chronoamperometric Analysis

The material was subjected to amperometric analysis potentiostat (Autolab, PGSTAT-30) with a frequency analyzer to determine the sensing response over time. The amount of silver-doped zinc oxide nanoparticles combined with the graphite powder to make a fine powder influences the efficiency of the working electrode. Ag-ZnO nanoparticles have been employed as oxidation probes.

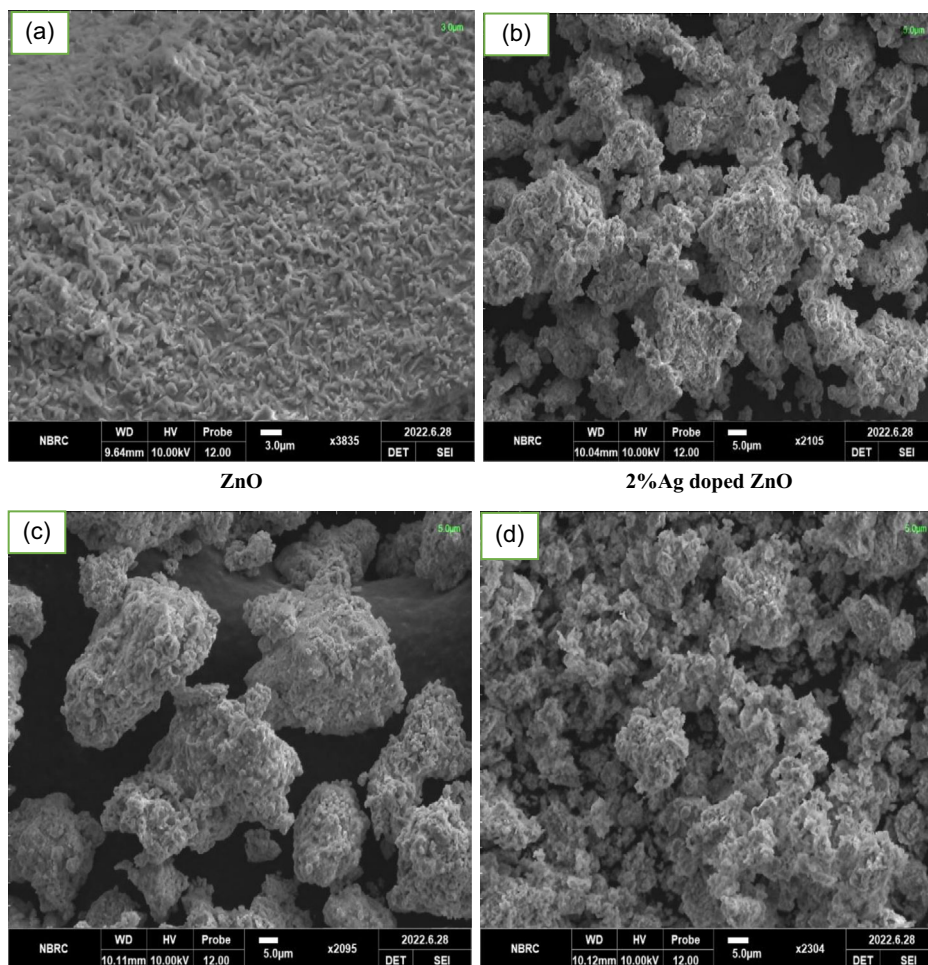


**Figure 5.** SEM analysis: a) ZnO, b) 2% Ag-doped ZnO, c) 3% Ag-doped ZnO, and d) 4% Ag-doped ZnO.

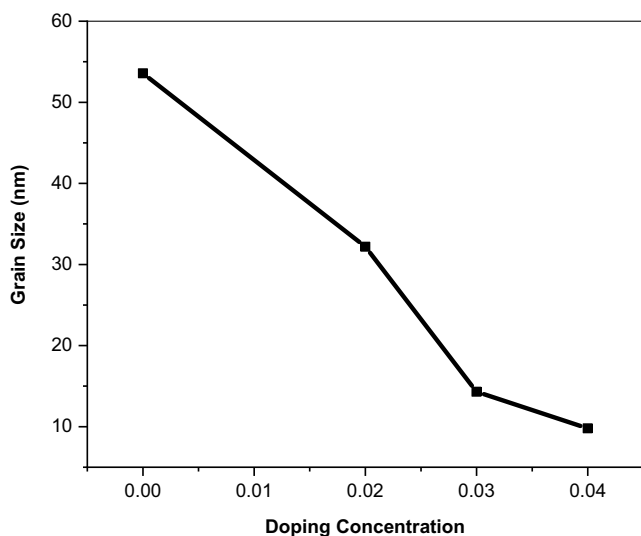


**Figure 6.** Doping concentration vs grain size.

Ferricyanide has been used as a supporting electrolyte to evaluate the redox potential of modified electrodes. The electron transport kinetics of each sample were somewhat different. The sequential addition of hydrogen peroxide played an enzymatic role, and the data were recorded at potentials of +0.5 and -0.2 V, which were used to measure the  $H_2O_2$  oxidation signals of the glucose level. The redox peaks indicate the electrochemical behavior of the pure zinc oxide nanoparticles and the remaining three silver-doped zinc oxide samples. An increase in the conducting capacity and catalytic ability of the Ag-ZnO-modified electrode was observed as cited in **Figure 7**.

The electron transfer of the Ag-ZnO-modified electrode increased with the coupling of the solution and electrode. The number of electroactive sites at the electrodes increased due to silver doping. The four modified electrodes were prepared relative to the ZnO 2% Ag-doped ZnO, 3% Ag-doped ZnO, and 4%

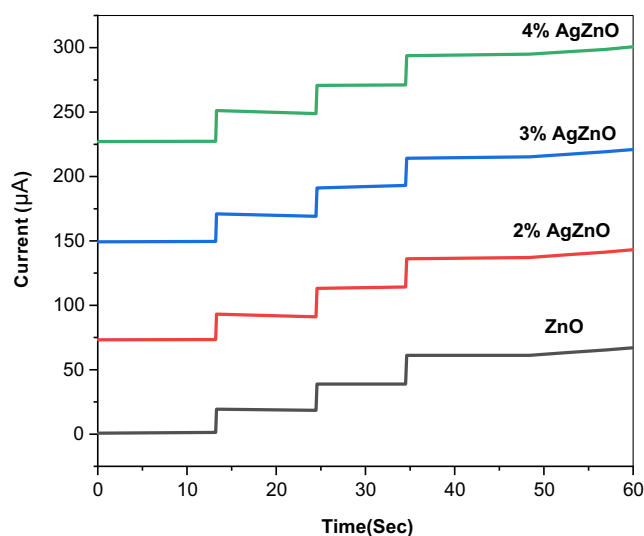


**Figure 7.** Amperometric behavior of ZnO and Ag-doped ZnO.

Ag-doped ZnO. The potential of the working electrodes was assessed via a multistep chronoamperometry approach. The scan rate was maintained at  $50 \text{ mV s}^{-1}$  to estimate glucose. The response time increased exponentially with increasing current intensity. When a substantial amount of glucose was present, the 4% Ag-doped ZnO generated a pattern with a high current response peak. The oxidation and intensity peak of ZnO was the lowest among the samples. The amperometric findings in this work were consistent with those of past studies.

The electroactive surface area was increased by silver doping. A similar inference was made in the present study because efficient electron transfer was observed in the Ag-ZnO-prepared electrode. Comparatively, the modified electrode seems more efficient than the pure zinc oxide-prepared electrode. This means that the number of active sites on the Ag-ZnO-modified electrode increased.<sup>[15]</sup> Integrating Ag into the zinc oxide structure is favorable because zinc oxide is an n-type semiconductor. However, Ag is a p-type impurity. Hence, Ag doping constructively favors the development of p-type zinc oxide semiconductors.<sup>[22]</sup> Silver successfully occupies the oxygen vacancies in the structure of ZnO. Silver doping smooths the surface of ZnO, reducing the degree of randomness. When the dopant is coated on the carbon fiber electrode, the surface becomes smooth and promotes a uniform orientation. Increasing the value of the dopant significantly increased the current response with time.<sup>[21,23]</sup> In a similar context, the performance of the ZnO-based glucose biosensor was improved with silver doping, which increased the electrocatalytic efficiency for glucose oxidation in the present work.

### 3.7. Temperature-Dependent Chronoamperometric Analysis

The sensing properties of the ZnO and Ag-doped ZnO samples are shown in **Figure 8**, which reveals that they have good sensitivity and response times with respect to temperature. Figure 8 shows the low response of the 5 mM glucose solution with the ZnO sample compared with the 2%, 3%, and 4% samples as the temperature increased. This result indicates that silver doping

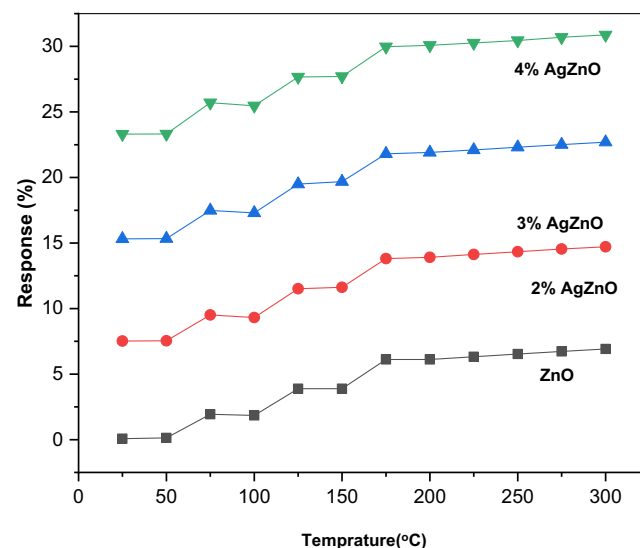


**Figure 8.** Sensing response vs. temperature.

and precipitated silver ions can improve the response at temperatures ranging from 0 to 300 °C. Ag doping improved the sensing properties of ZnO and Ag-doped ZnO with increasing temperature when the electrodes were exposed to a 5 mM glucose solution, and the best sensitivity was achieved with the sample with 4% Ag-doped ZnO as shown in Figure 8.

Enhance electron mobility, reducing impedance with increasing temperature at the range of 200–300 °C Enhances electrochemical activity, increasing current density. Ag-doped ZnO increases Current density increases with temperature and with optimal performance at 200–300 °C.

### 3.8. The Electrochemical Impedance Spectroscopy

The Nyquist curve of ZnO indicates high impedance and low conductivity due to high charge transfer resistance and low electron transfer process via potentiostat (Autolab, PGSTAT-30) with a frequency analyzer. In the case of Ag-doped ZnO, a decrease in the curve is reported, as well as an increased conductivity response because of the increased electron transfer rate. It is also reported in Figure 9 that the curve becomes low with the increasing Ag concentration which enhanced electrochemical performance, increased conductivity, and also improved electron transfer. The decrease in the curve with Ag concentration is evidence of reduced impedance and increases the sensing response toward glucose.

The all-impedance measurements are observed at room temperature as it is also cited in Figure 8 that the sensing response toward glucose increases with temperature, because at high temperature the Nyquist curve decreases and it also decreases with the Ag concentration due to increased surface area enhancing glucose molecule adsorption, improved electron transfer facilitating glucose oxidation, and increased conductivity reducing response time.

### 3.9. Sensing Response

The glucose oxidation peak typically appears between 0.4 and 0.6 V (versus Ag/AgCl) in electrochemical measurements, such as cyclic voltammetry (CV) or amperometry. This potential range

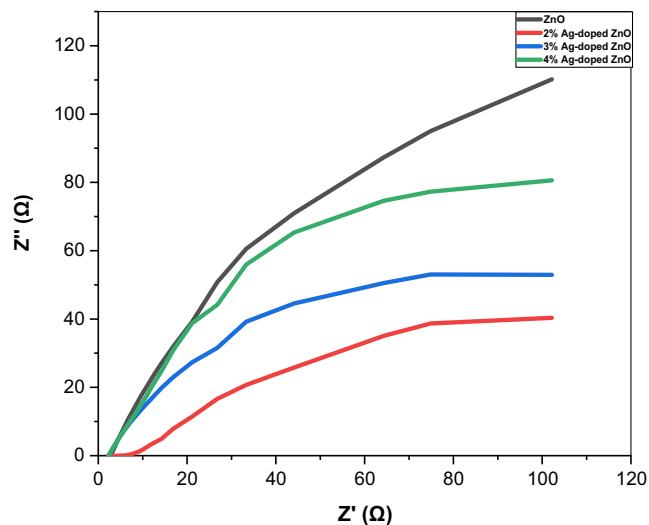


Figure 9. The Nyquist Graph of all samples.

corresponds to the oxidation of glucose to gluconic acid, which is catalyzed by glucose oxidase (GOx) enzyme.

GOx catalyzes the oxidation of glucose to gluconic acid, producing hydrogen peroxide (H<sub>2</sub>O<sub>2</sub>) as a byproduct. The glucose oxidation reaction occurs at the electrode surface, typically made of platinum, gold, or carbon materials. The potential range of 0.4–0.6 V is optimal for glucose oxidation, as it allows for efficient electron transfer between the enzyme and the electrode.

Factors influencing the glucose oxidation peak potential are pH, temperature, electrode material and surface modification, GOx enzyme loading and activity, and glucose concentration.

A silver-doped zinc oxide-modified electrode was used to determine the effects of the presence and absence of interfering species on the electrochemical behavior of the electrode in a glucose solution. Initially, glucose was detected by the prepared electrode. The scan rate of the CV was maintained at 50 mV s<sup>-1</sup>. As shown in Figure 10, only oxidation peaks were observed via CV. When glucose was present, the increased electron transfer and surface activation phenomena increased the peak intensity. A higher current response was given by the Ag-doped ZnO-amended electrode in the presence of glucose. When glucose was added to the buffer solution, the electrochemical reaction of the Ag-doped ZnO-modified electrode was observed by keeping the scan rate of CV constant. Owing to its reversibility and very rapid electron transfer rate, the Ag-doped ZnO-modified electrode strongly improved the electrocatalytic process with glucose.

Dynamic changes in resistance and the glucose-sensing response are used to evaluate glucose-sensing characteristics. Initially, the 4% Ag-doped ZnO sensors were exposed to a 5 mM glucose solution. To find the better condition to get response toward glucose sensor with high accuracy and stability. Figure 10 shows the dynamic response of the 4%Ag-doped ZnO sensor to a 5 mM solution of glucose, which is a typical response of n-type oxides, and the resistance decreases upon exposure to reducing or increasing the c concentration of the glucose solution.

Doped ZnO can exhibit improved stability due to the presence of Ag, which can reduce the reactivity of ZnO with moisture and oxygen. It also enhances the thermal stability of ZnO.

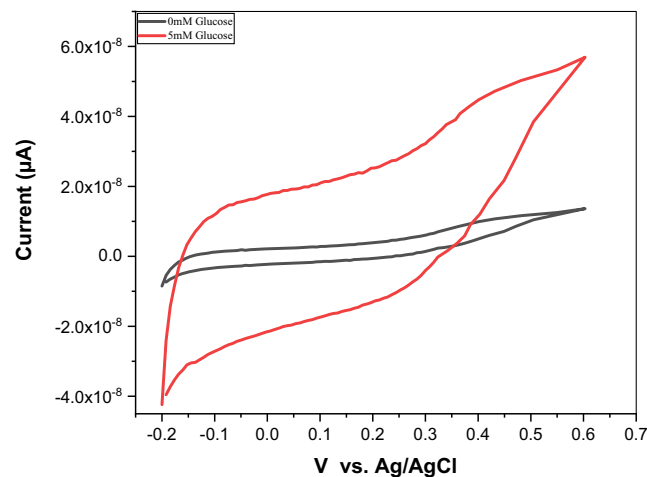


Figure 10. Sensing response toward glucose.

Homogeneity refers to the uniform distribution of components within the material. In the case of Ag-doped ZnO, homogeneity is crucial to ensure consistent properties.<sup>[24–29]</sup>

ZnO's high surface-to-volume ratio and Ag doping improve the sensitivity of glucose detection. ZnO and Ag-doped ZnO can be functionalized to selectively detect glucose in the presence of other sugars. ZnO's stability and Ag doping enhance the sensor's durability and resistance to interference. ZnO and Ag-doped ZnO-based sensors can detect glucose at low concentrations, making them suitable for diabetes management. The sensors exhibit rapid response times, enabling real-time glucose monitoring. ZnO and Ag-doped ZnO-based sensors can detect glucose without enzymes, reducing costs and improving shelf life.

Ag doping enhances the glucose sensing performance by increasing the surface area, improving the electron transfer rate, and enhancing the binding affinity for glucose molecules. The combination of ZnO and Ag doping creates a highly sensitive, selective, and stable glucose sensor, making it an attractive material for diabetes management and monitoring applications.<sup>[30–33]</sup>

#### 4. Conclusion

In summary, monitoring blood sugar several times a day is promising for the successful management of diabetes. In this study, a conducive and well-grounded approach was followed to fabricate a nonenzymatic glucose biosensor. The enormous potential of silver-doped ZnO nanoparticles was clearly evident in the outcomes. The sol-gel synthesis of pure and Ag-doped ZnO nanoparticles yields a good product. The potential of Ag-doped ZnO nanoparticles in glucose sensing has been estimated by the use of a three-electrode system. The semiconductor and electrocatalytic properties of ZnO NPs have been enhanced by Ag doping. The excellent performance of the developed system was due to the enhanced electron-mediating properties of Ag-ZnO-NPs. The contrasting studies with different objectives corroborate the current outcomes. The additional phases were evident in the FTIR spectrum because silver doping generates Ag–O and Ag–O<sub>2</sub> bonds. The SEM results revealed a tiny hexagonal nanorod morphology in the pure and doped samples, with no significant change in the crystal dimensions. SEM revealed symmetrically organized hexagonal nanorods in the prepared samples, and the morphology of the rods increased with increasing scan rate. The average grain size of the sample was calculated to be 27.46 nm via ImageJ software. The UV-absorption spectrum revealed that the sample with a high silver concentration (4% Ag-ZnO-NPs) has less significant optical properties in the visible region. The maximum absorbance of ZnO is observed around 370 nm, which corresponds to the UV region, in the case of 4% Ag doping introducing LSPR effects, leading to increased absorbance in the visible region 536 nm. The absorption peak in the UV region shifts to longer wavelengths (e.g., 380–400 nm) due to the introduction of Ag-related energy levels. The secondary phases (Ag–O, Ag–O<sub>2</sub>) were evident in the FTIR spectrum of the doped samples. The amperometric behavior of the 4% Ag-ZnO-NP-modified electrode shows the highest response to current and generates the highest response peak in the plot. The Nyquist curve confirmed the improvement of the

chronometric current toward glucose with temperature. The sensing response of the 4% Ag-ZnO-NP-modified electrode at a scan rate of 50 mV s<sup>-1</sup> (measured from -0.2 to +0.5 V) was the highest. The response toward glucose is observed to improve with temperature. This was an indication of an increase in electroactive sites due to silver doping; silver doping facilitated the oxidation of electrons and generated the highest response peak in the chronoamperometry plot. Overall, this work paves the way for the use of prepared metal oxide nanomaterials for transporting electrons in advanced nonenzymatic glucose biosensing systems.

#### Acknowledgements

The authors extend their appreciation to King Saud University for funding this work through the Researchers Supporting Project number (RSP2024R378), King Saud University, Riyadh, Saudi Arabia.

#### Conflict of Interest

The authors declare no conflict of interest.

#### Data Availability Statement

The data that support the findings of this study are available from the corresponding author upon reasonable request.

#### Keywords

chronoamperometry, glucose monitoring, silver-doped zinc oxide nanoparticles, sol-gel processes, zinc oxide

Received: October 12, 2024

Revised: October 14, 2024

Published online:

- [1] J. Zhuang, H. Pan, W. Feng, *Materials* **2024**, *6*, 6005.
- [2] X. Xiao, Q. He, Z. Li, A. O. Antoce, X. Zhang, *Food Control* **2017**, *73*, 1556.
- [3] H. Yang, J. Zheng, W. Wang, J. Lin, J. Wang, L. Liu, Y. Liao, *Adv. Sci.* **2024**, *11*, 2405848.
- [4] C. Zhao, X. Tang, J. Zhao, J. Cao, Z. Jiang, J. Qin, *J. Nanobiotechnol.* **2022**, *20*, 507.
- [5] Z. Jiang, X. Han, C. Zhao, S. Wang, X. Tang, *Int. J. Mol. Sci.* **2022**, *23*, 1923.
- [6] Q. Wang, X. Xiang, B. Chen, *Curr. Opin. Food Sci.* **2024**, *56*, 101134.
- [7] L. Zhu, C. Ma, W. Li, M. Huang, W. Wu, C. S. Koh, F. Blaabjerg, *IEEE Transactions on Energy Conversion*, Vol. 39, IEEE, Piscataway, NJ **2024**, pp. 1726–1737.
- [8] Y. Chuai, B. Dai, X. Liu, Y. Chuai, B. Dai, X. Liu, M. Hu, Y. Wang, H. Zhang, *BMC Oral Health* **2023**, *23*, 303.
- [9] Z. Wang, W. Sun, R. Hua, Y. Wang, Y. Li, H. Zhang, *Int. J. Oral Sci.* **2024**, *16*, 24.
- [10] W. Zhang, Y. Zhang, C. Jin, R. Fang, R. Hua, X. Zang, H. Zhang, *Eur. J. Med. Res.* **2023**, *28*, 287.
- [11] Y. Wang, W. Wu, M. Christelle, M. Sun, Z. Wen, Y. Lin, H. Zhang, J. Xu, *Eur. J. Med. Res.* **2024**, *29*, 84.
- [12] X. Liu, B. Dai, Y. Chuai, Y. Chuai, M. Hu, H. Zhang, *Clin. Oral Invest.* **2023**, *27*, 4727.

- [13] S. Al-Ariki, N. A. A. Yahya, S. A. Al-A'nsi, M. H. H. Jumali, A. N. Jannah, R. Abd-Shukor, *Sci. Rep.* **2021**, *11*, 11948.
- [14] T. Chitradevi, A. Jestin Lenus, N. Victor Jaya, *Mater. Res. Express* **2020**, *7*, 015011.
- [15] C. Erdem, D. K. Zeybek, G. Aydoğdu, B. Zeybek, S. Pekyardımcı, E. Kılıç, *Artif. Cells Nanomed. Biotechnol.* **2014**, *42*, 237.
- [16] J. Narang, N. Chauhan, P. Jain, C. S. Pundir, *Int. J. Biol. Macromol.* **2012**, *50*, 672.
- [17] G. N. Dar, A. Umar, S. Abbas Zaidi, S. Baskoutas, S. H. Kim, M. Abaker, A. Al-Hajry, S. A. Al-Sayari, *Talanta* **2012**, *89*, 155.
- [18] R. Zeferino, M. Barboza-Flores, U. Pal, *J. Appl. Phys.* **2011**, *109*, 014308.
- [19] T. Jan, J. Iqbal, M. Ismail, A. Mahmood, *J. Appl. Phys.* **2014**, *115*.
- [20] M. E. Ashebir, G. M. Tesfamariam, G. Y. Nigussie, T. W. Gebreab, *J. Nanomater.* **2018**, *2018*, 9425938.
- [21] F. Zhou, W. Jing, P. Liu, D. Han, Z. Jiang, Z. Wei, *Sensors* **2017**, *17*.
- [22] I. Khan, K. Saeed, I. Khan, *Arabian J. Chem.* **2019**, *12*, 908.
- [23] M. Junaid, R. Jabeen, S. A. Buzdar, W. Q. Khan, M. Anwar, M. Javed, F. Warsi, *Iron-doped Nickel Oxide as a Potential Biosensor of Urea Determination via Voltammetry* **2023**, <https://doi.org/10.1016/j.physb.2022.414592>.
- [24] O. M. Ikumapayi, E. T. Akinlabi, A. O. M. Adeoye, S. O. Fatoba, *Mater. Today: Proc.* **2021**, *44*, 1154.
- [25] V. Naresh, N. Lee, *Sensors* **2021**, *21*, 1109.
- [26] N. Pal, D. Chakraborty, B. E. Cho, G. J. Seo, *Nanomaterials* **2023**, *13*, 2184.
- [27] A. M. Abu-Dief, *J. Nanotechnol. Nanomater.* **2020**, *1*.
- [28] M. Junaid, S. G. Hussain, N. U. Ain, R. Jabeen, W. Q. Khan, N. Abbas, *J. Nanoscope* **2022**, *3*, 29.
- [29] T. Bharat, S. Mondal, H. Gupta, P. Singh, A. Das, *Mater. Today: Proc.* **2019**, *11*, 767.
- [30] A. K. Azfar, M. F. Kasim, I. M. Lokman, H. A. Rafaie, M. S. Mastuli, *Royal Soc. Open Sci.* **2020**, *7*, 191590.
- [31] A. Mahmoud, *Molecules* **2021**, *26*, 929.
- [32] K. Phasuksom, A. Sirivat, *RSC Adv.* **2022**, *12*, 28505.
- [33] A. Q. Ahmad, N. Attique, R. Ali, W. Abbas, M. Nadeem, M. Junaid, N. Ul Ain, *Flavus, Results Chem.* **2024**, *7*, 101312.